moving target. Of course, we cannot generalise our results, as this study was limited to 2 patients.

One of the advantages of IBPR is that no extra devices are required. It also provides direct tracking of tumour motion in contrast to methods that require external devices. In addition, correlations in the motion of inner structures and the body surface are not always measurable by external devices [15]. This is a critical problem for 4D-CT reconstruction.

In addition to our NCC method, several IBPR techniques such as the Amsterdam shroud method [11,12] and Kavanagh's method [13] have been proposed to acquire respiratory signals for kV projection images. The former projects 2D images onto the cranio-caudal axis to obtain a 1D signal for each image, while the latter utilises changes in the pixel value summation within each projection image. Both methods are based on pixel value projection and are easily affected by MLC motion, which yields drastic changes in pixel values within the projection images even if the MLC motion is as small as it was in our cases. Therefore, these methods would have difficulty with portal images.

Current issues or limitations of VMAT-CBCT reconstruction include the influence of intensity distribution and the shape yielded by MLC on the projection images. We performed a homogeneous correction of the total intensity within a field depending on the size and monitor unit. However, the change in field size yields an inhomogeneous intensity within the field, a matter that must be addressed in future studies. In addition, due to limitations of the Elekta iView software, the maximum number of portal imaging sequential acquisitions is only 256, so the acquisition of images may be insufficient for longer treatments. For stable P-IBPR, a sampling interval should be short enough to acquire a respiratory signal. Therefore, in this study, the shortest sampling rate of the Elekta iView software was employed, and the portal imaging was performed during less than half of a gantry rotation.

The inhomogeneous value inside the insert of the phantom as seen in Fig. 5 was also partly caused by this limitation. Optimised operation for the acquisition of portal images should be allowed in the system. Alternatively, a reconstruction algorithm can be developed as represented by digital tomosynthesis [16,17] and by compressed sensing [18] for a limited acquisition angle. The removal of such problems will enable quantitative derivation of 4D VMAT-CBCT.

In conclusion, a 4D VMAT-CBCT reconstruction technique was developed by using P-IBPR with the NCC method, which enabled us to obtain in-treatment volume images in 4 phases. The visibility of the anatomy in 4D VMAT-CBCT reconstruction for lung cancer patients makes this a promising tool for verifying relative tumour positions for each respiratory phase.

Acknowledgements

This work was partially supported by JSPS KAKENHI 22791176. S.K. and A.H. wish to thank Dr. Grant Jackson (Elekta K.K.) for his advice regarding the use of iCom to acquire log data during treatment. K.N. received research funding from Elekta K.K.

References

[1] van Elmpt W, McDermott L, Nijsten S, et al. A literature review of electronic portal imaging for radiotherapy dosimetry. Radiother Oncol 2008;88:289–309.
[2] Nijsten SM, Mijnheer BJ, Dekker AL, et al. Routine individualized patient dosimetry using electronic portal imaging devices. Radiother Oncol 2007;83:65–75.
[3] McDermott LN, Wendling M, Sonke JJ, et al. Replacing pretreatment verification with in vivo EPID dosimetry for prostate IMRT. Int J Radiat Oncol Biol Phys 2007;67:1568–77.
[4] Murphy MJ, Balter J, Balter S, et al. The management of imaging dose during image-guided radiotherapy: report of the AAPM Task Group 75. Med Phys 2007;34:4041–6063.
[5] Balter J, Benedict S, Bissonnette JP, et al. The role of in-room kV X-ray imaging for patient setup and target localization, AAPM Report No. 104. American Association of Physics in Medicine, 2009.
[6] Nakagawa K, Yamashita H, Shiraishi K, et al. Verification of in-treatment tumour position using kilovoltage cone-beam computed tomography: a preliminary study. Int J Radiat Oncol Biol Phys 2007;69:970–3.
[7] Nakagawa K, Haga A, Shiraishi K, et al. First clinical cone-beam CT imaging during volumetric modulated arc therapy. Radiother Oncol 2009;90:422–3.
[8] Ling C, Zhang P, Etmektzoglou T, et al. Acquisition of MV-scatter-free kilovoltage CBCT images during RapidArc™ or VMAT. Radiother Oncol 2011;100:145–9.
[9] Nakagawa K, Kida S, Haga A, et al. Cone beam computed tomography data acquisition during VMAT delivery with subsequent respiratory phase sorting based on projection image cross-correlation. J Radiat Res (Tokyo) 2011;52:112–3.
[10] Poludniowski G, Thomas MDR, Evans PM, et al. CT reconstruction from portal images acquired during volumetric-modulated arc therapy. Phys Med Biol 2011;55:5635–51.
[11] Sonke JJ, Zijp L, Remeijer P, van Herk M. Respiratory correlated cone beam CT. Med Phys 2005;32:1176–86.
[12] Zijp L, Sonke J, van Herk M. Extraction of the respiratory signal from sequential thorax cone-beam X-ray images. Jeong Publishing (Seoul) 2004:507–9.
[13] Kavanagh A, Evans PM, Hansen VN, et al. Obtaining breathing patterns from any sequential thoracic X-ray image set. Phys Med Biol 2009;54:4879–88.
[14] Otani Y, Fukuda I, Tsukamoto N, et al. A comparison of the respiratory signals acquired by different respiratory monitoring systems used in respiratory gated radiotherapy. Med Phys 2010;37:6178–86.
[15] Korreman SS, Juhler-Nottrup T, Boyer AL. Respiratory gated beam delivery cannot facilitate margin reduction, unless combined with respiratory correlated image guidance. Radiother Oncol 2008;86:61–8.
[16] Maurer J, Godfrey D, Wang Z, et al. On-board four-dimensional digital tomosynthesis: first experimental results. Med Phys 2008;35:3574–83.
[17] Maurer J, Pan T, Yin FF. Slow gantry rotation acquisition technique for on-board four-dimensional digital tomosynthesis. Med Phys 2010;37:921–33.
[18] Choi K, Wang J, Zhu L, et al. Compressed sensing based cone-beam computed tomography reconstruction with a first-order method. Med Phys 2010;37:5113–25.

Technical Note: Extension of van Herk's treatment margin model for anisotropic systematic positioning errors in Cartesian coordinate system[a)]

Kiyoshi Yoda[b)]
Elekta KK, 3-9-1 Shibaura, Minato-ku, Tokyo 108-0023, Japan

Keiichi Nakagawa
Department of Radiology, University of Tokyo Hospital 7-3-1 Hongo, Bunkyo-ku, Tokyo 113-8655, Japan

(Received 11 April 2011; revised 6 May 2011; accepted for publication 10 May 2011; published 16 June 2011)

Purpose: A coefficient of a treatment margin model for anisotropic systematic positioning errors has been calculated in Cartesian coordinate system based on van Herk's analytical formulation.
Methods: Three-dimensional (3D) patient population distribution was formulated in Cartesian coordinate system to model anisotropic systematic positioning errors. Analytical 3D integration with anisotropic standard deviations Σ's and the following Newton's method yielded the coefficient of van Herk's systematic positioning error model in Cartesian coordinate system.
Results: The treatment margins for the anisotropic systematic errors in Cartesian coordinate system were 2.1 Σ for 90% patient population coverage and 2.4 Σ for 95% patient population coverage.
Conclusions: It was found that the treatment margins for anisotropic systematic positioning errors in Cartesian coordinate system were smaller than those for the isotropic model in spherical coordinate system for a given patient population coverage probability. © *2011 American Association of Physicists in Medicine.* [DOI: 10.1118/1.3596531]

Key words: treatment margin, Cartesian coordinate system, systematic positioning errors

Marcel van Herk *et al.* proposed an analytical treatment margin model that considered both systematic positioning errors among all the patients in a facility and random positioning errors among all the treatment fractions for each patient.[1,2] The coefficients of the model parameters were numerically calculated under a spherically symmetric condition thereby leading to an isotropic margin perpendicular to a spherical tumor surface. However, recent high precision treatment is performed under Cartesian coordinate system with a 3 or 6 degrees-of-freedom couch, and the systematic positioning errors may be anisotropic. Although the original article mentioned an extension to anisotropic modeling,[1] detailed results have not been published.

In this article, three-dimensional (3D) Gaussian patient population is formulated in Cartesian coordinate system to model anisotropic systematic errors for patient positioning. Analytical integration with anisotropic standard deviations and the following Newton's method are performed to derive the coefficient of van Herk's systematic positioning error model in Cartesian coordinate system.

The 3D Gaussian patient population model is given by

$$G(x,\Sigma_x^2)G(y,\Sigma_y^2)G(z,\Sigma_z^2), \tag{1}$$

where $G(r,\Sigma_r^2)$ denotes the probability density of one-dimensional Gaussian distribution with a standard deviation of Σ_r, where r is x, y, or z. For example, $G(x,\Sigma_x^2)$ is given by

$$G(x,\Sigma_x^2) = \frac{e^{-\frac{x^2}{2\Sigma_x^2}}}{\sqrt{2\pi}\Sigma_x}. \tag{2}$$

The coverage probability of the patient population in the systematic positioning error ranges of $-c\ \Sigma_x < x < c\ \Sigma_x$, $-c\ \Sigma_y < y < c\ \Sigma_y$, and $-c\ \Sigma_z < z < c\ \Sigma_z$ is given by 3D integration of (1) leading to

$$\mathrm{erf}\left(\frac{c}{\sqrt{2}}\right)^3 \tag{3}$$

where c is an arbitrary positive constant, and erf is the error function. The analytical integration was performed by a computer code, Mathematica,[3] as shown in Fig. 1.

The expression (3) is a trivial form because it is the third power of the one-dimensional result shown in van Herk's paper,[1] however, to the author's knowledge it has not been calculated nor compared to the original van Herk's coefficient in spherical coordinate system. To solve the nonlinear equation, Newton's method was employed and the results are shown in Table I. Again, the numerical root finding was performed by Mathematica,[3] which is also shown in Fig. 1. It was found that the treatment margins for anisotropic systematic positioning errors in Cartesian coordinate system were smaller than those for the isotropic model in spherical coordinate system for a given patient population coverage probability.

In conclusion, van Herk's treatment margin model for systematic errors was reformulated by calculating the coefficient of the anisotropic systematic error model in Cartesian coordinate system. The resulting coefficient was smaller than that for the spherically symmetric model.

Further modification would be possible by integrating (1) with varied integration ranges in 3D directions. Meanwhile,

```
gaussian3Danisotropic =
  Function[{x, y, z},
          Exp[-x^2 / (2 sigmax^2)] / sigmax / Sqrt[2 Pi] *
          Exp[-y^2 / (2 sigmay^2)] / sigmay / Sqrt[2 Pi] *
          Exp[-z^2 / (2 sigmaz^2)] / sigmaz / Sqrt[2 Pi]
  ]
```

$$\text{Function}\left[\{x, y, z\}, \frac{e^{-\frac{x^2}{2\,\text{sigmax}^2}}\, e^{-\frac{y^2}{2\,\text{sigmay}^2}}\, e^{-\frac{z^2}{2\,\text{sigmaz}^2}}}{(\text{sigmax}\sqrt{2\pi})\,(\text{sigmay}\sqrt{2\pi})\,(\text{sigmaz}\sqrt{2\pi})}\right]$$

```
Integrate[
  gaussian3Danisotropic[x, y, z],
    {x, -Infinity, Infinity}, {y, -Infinity, Infinity}, {z, -Infinity, Infinity},
      Assumptions → {sigmax > 0, sigmay > 0, sigmaz > 0}
]
```

```
1
```

```
Integrate[
  gaussian3Danisotropic[x, y, z],
    {x, -c sigmax, c sigmax}, {y, -c sigmay, c sigmay}, {z, -c sigmaz, c sigmaz}
]
```

$$\text{Erf}\left[\frac{c}{\sqrt{2}}\right]^3$$

$$\text{FindRoot}\left[\text{erf}\left(\frac{c}{\sqrt{2}}\right)^3 = 0.8, \{c, 1.\}\right]$$

```
{c → 1.80113}
```

$$\text{FindRoot}\left[\text{erf}\left(\frac{c}{\sqrt{2}}\right)^3 = 0.85, \{c, 1.\}\right]$$

```
{c → 1.93711}
```

$$\text{FindRoot}\left[\text{erf}\left(\frac{c}{\sqrt{2}}\right)^3 = 0.9, \{c, 1.\}\right]$$

```
{c → 2.11405}
```

$$\text{FindRoot}\left[\text{erf}\left(\frac{c}{\sqrt{2}}\right)^3 = 0.95, \{c, 1.\}\right]$$

```
{c → 2.38774}
```

$$\text{FindRoot}\left[\text{erf}\left(\frac{c}{\sqrt{2}}\right)^3 = 0.99, \{c, 1.\}\right]$$

```
{c → 2.93416}
```

FIG. 1. A computer code for calculating the coefficient of van Herk's treatment margin model for anisotropic systematic positioning errors in Cartesian coordinate system. Each bold part is a command followed by each calculated result.

TABLE I. Treatment margins, $\alpha\,\Sigma$, for systematic positioning errors as a function of patient population coverage probability.

Patient population coverage (%)	Cartesian 3D model (Σ)	Spherical 3D model (Σ)
80	1.80	2.16
85	1.94	2.31
90	2.11	2.50
95	2.39	2.79
99	2.93	3.36

the present author believes that the most important point to keep in mind is that the present margin model excludes delineation errors in a clinical target volume.[1,2,4]

[a]Dr Nakagawa receives research funding from Elekta.
[b]Electronic mail: Kiyoshi.Yoda@elekta.com

[1]M. van Herk, P. Remeijer, C. Rasch, and J. V. Lebesque, "The probability of correct target dosage: Dose-population histograms for deriving treatment margins in radiotherapy," Int. J. Radiation Oncology Biol. Phys. **47**, 1121–1135 (2000).
[2]M. van Herk, "Errors and margins in radiotherapy," Semin. Radiat. Oncol. **14**, 52–64 (2004).
[3]S. Wolfram, *Mathematica, a System for Doing Mathematics by Computer* (Addison-Wesley, San Francisco, 1991).
[4]M. van Herk, "Will IGRT live up to its promise?," Acta Oncol. **47**, 1186–1187 (2008).

J. Radiat. Res., 52, 536–537 (2011)

First In-situ Dose Calculation Report Using In-treatment Kilovoltage Cone-beam CT and In-treatment Linac Parameters during Volumetric Modulated Arc Therapy

Akira SAKUMI[1], Akihiko HAGA[1], Satoshi KIDA[1], Naoya SAOTOME[1], Yukari OKANO[1], Kenshiro SHIRAISHI[1], Takeshi ONOE[1], Kiyoshi YODA[2], Kuni OHTOMO[1] and Keiichi NAKAGAWA[1]*

In-situ dose calculation/In-treatment cone-beam CT/Volumetric modulated arc therapy.

To the editor

Tumor registration using kilovoltage (kV) cone-beam CT (CBCT) prior to radiotherapy has been increasingly adopted for daily clinical practice. Compared to traditional two-dimensional bone registration, kV CBCT provides three-dimensional tumor registration between previously acquired planning CT and the CBCT on each treatment day. In addition, kV CBCT shows daily displacement and deformation of organs as well as regression of tumors during the course of the treatment.

As a natural next step, patient dose distribution on each treatment day has been gradually highlighted by using CBCT image data. The reported accuracy of the CBCT-based dose calculation in reference to a planning CT was within 2 to 3%.[1,2] In the meantime, we have already reported clinical kV CBCT imaging during rotational radiotherapy using a linac with a CBCT unit (Elekta, UK)[3] and volumetric modulated arc therapy (VMAT).[4] We also published a dose calculation procedure by referring to log files including actual data of multi leaf collimator (MLC) positions, jaw positions, gantry angles and MUs with an interval of every 0.25 seconds in the linac service mode.[5] Recently, Qian calculated dose distributions by combining CBCT images acquired before treatment and actual in-treatment log files stored in a Varian linac.[6] In contrast, we report the first in-situ dose calculation using in-treatment CBCT and in-treatment linac parameters during VMAT delivery, which may directly correspond to the actually absorbed dose distributions during treatment.

A treatment planning system (TPS), Pinnacle3 9.0 SmartArc (Phillips, Holland) was employed to create a single-arc VMAT plan for a prostate cancer patient. The PTV dose prescription (D_{95}) was 76 Gy in 38 fractions. The linac photon energy was 6 MV. A record and verify system, Mosaiq 1.6 (Elekta, USA), was employed with a linac control software, Desktop Pro 7.0.1 (Elekta, UK). A single-arc VMAT required approximately 120 seconds. During the VMAT delivery, a log file was recorded via iCOM interface (Elekta, UK). Subsequently, the iCom data format was converted to Pinnacle data format, thereby allowing Pinnacle to read actual MLC positions, jaw positions, gantry angles and MUs with an interval of every 0.25 seconds. During the VMAT delivery, in-treatment kV projection data were also stored and CBCT image reconstruction was performed by in-house software. By exporting these data back to the TPS, in-treatment dose distributions were obtained.

Figure 1(a) shows the resulting in-situ dose distribution calculated by the in-treatment CBCT and the in-treatment linac parameters. The innermost two contours are clinical target volume (CTV) and planning target volume (PTV) of the prostate cancer. A PTV margin of 5 mm was employed except for the rectum side with a 4 mm margin. The isodose contour lines are, from inside to outside, 107% (a tiny blue island near the PTV boundary), 95%, 90%, 80%, 70%, 60%, 50%, 30% and 10% (purple) of the prescribed dose. A CBCT value to density conversion table was created by referring to a planning CT value to density table at the corresponding pixel locations on the paired data set of the planning CT and the CBCT, in regions close to the PTV including prostate, fat, and bone anatomies. To reduce scattering effects, CBCT values were corrected, with a simple approximation, based on a reconstructed CBCT image of a water column phantom, where a non-linear correction function was determined as a function of radius from the image center. The calculated mean doses for the PTV and rectum using the planning CT and the CBCT agreed within 1.4% and 3.4%, respectively. Figure 1(b) shows in-situ isodose color map overlaid on the in-treatment CBCT image, and Fig. 1(c) shows dose distributions calculated by the planning

*Corresponding author: Phone: +81-3-5800-8786,
Fax: +81-3-5800-8786,
E-mail: k-nak@fg7.so-net.ne.jp
[1]Department of Radiology, University of Tokyo Hospital, 7-3-1 Hongo, Bunkyo-ku, Tokyo, 113-8655, Japan; [2]Elekta KK, 3-9-1 Shibaura, Minato-ku, Tokyo 108-0023, Japan.
doi:10.1269/jrr.11061

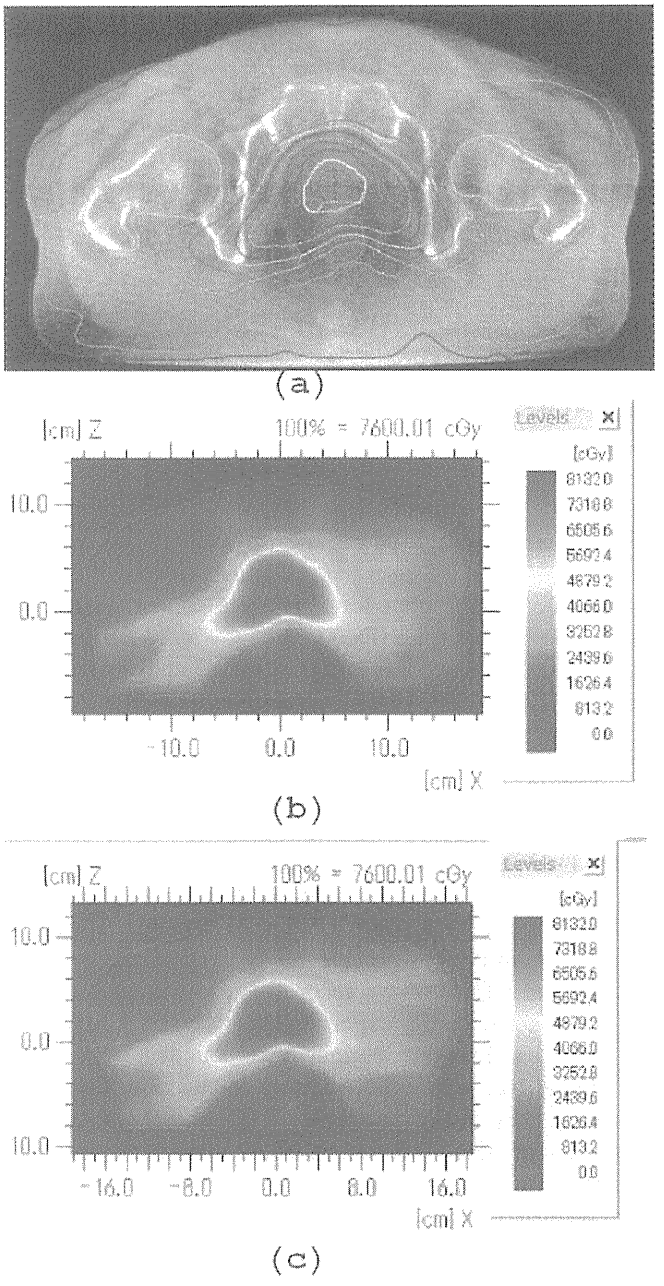

Fig. 1. In-situ dose calculation results using in-treatment cone-beam CT and in-treatment linac parameters during volumetric modulated arc therapy: (a) with isodose contours and (b) with isodose color map. An isodose color map calculated by the planning CT is shown in (c) for comparison.

CT for comparison. The pass rate of 1% dose difference between the dose distributions shown in (b) and (c) within the entire CBCT volume was 93.1%, whilst the pass rate of 2% dose difference went up to 96.5%. A reasonably good agreement was observed even if the body contour shapes were significantly different as shown at the both sides near the couch top.

In conclusion, we have shown that in-situ dose calculation during VMAT delivery is feasible by using in-treatment kV CBCT and in-treatment linac parameters. Further quantitative analysis is required to apply this technique to the next generation dose guided radiotherapy, which was originally proposed back in 2002.[7]

REFERENCES

1. Ding GX, *et al* (2007) A study on adaptive IMRT treatment planning using kV cone-beam CT. Radiother Oncol **85**: 116–125.
2. Richter A, *et al* (2008) Investigation of the usability of cone beam CT data sets for dose calculation. Radiation Oncology **3**: 42.
3. Nakagawa K, *et al* (2007) Verification of in-treatment tumor position using kilovoltage cone-beam computed tomography: preliminary study. Int J Radiat Oncol Biol Phys **69**: 970–973.
4 Nakagawa K, *et al* (2009) First clinical cone-beam CT imaging during volumetric modulated arc therapy. Radiother Oncol **90**: 422–423.
5. Haga A, *et al* (2009) Quality assurance of volumetric modulated arc therapy using Elekta Synergy. Acta Oncol **48**: 1193–1197.
6. Qian J, *et al* (2010) Dose reconstruction for volumetric modulated arc therapy (VMAT) using cone-beam CT and dynamic log files. Phys Med Biol **55**: 3597–3610.
7. Wu C, *et al* (2002) Re-optimization in adaptive radiotherapy. Phys Med Biol **47**: 3181–3195.

Received on April 11, 2011
Accepted on May 6, 2011

JOURNAL OF MEDICAL CASE REPORTS

CASE REPORT Open Access

Abscopal effect of radiation on lung metastases of hepatocellular carcinoma: a case report

Kae Okuma[1], Hideomi Yamashita[1*], Yuzuru Niibe[2], Kazushige Hayakawa[2], Keiichi Nakagawa[1]

Abstract

Introduction: The abscopal effect is the effect of radiation therapy at a site distant to the area of irradiation. This is not a common event and has not been clearly defined, resulting in few reported cases in the literature. We discuss this phenomenon in a patient with hepatocellular carcinoma.

Case presentation: A 63-year-old Japanese man underwent extended right hepatic lobectomy for hepatocellular carcinoma. During his follow-up examination, a single lung metastasis and a single mediastinal lymph node metastasis were found. Trans-catheter arterial embolization was initially attempted to treat the mediastinal tumor, however this approach failed to take effect and carried risks of spinal artery embolism. External-beam irradiation, with a dose of 2.25 Gy per fraction, was performed using an antero-posterior parallel-opposed technique (total dose, 60.75 Gy). A computed tomography scan performed one month after starting radiotherapy showed a remarkable reduction of the mediastinal lymph node metastasis. In addition to this, we observed spontaneous shrinking of the lung metastasis, which was located in the right lower lobe and out of the radiation field. No chemotherapy was given during the period. There has been no recurrence of either the lung metastasis or the mediastinal lymph node metastasis during a follow-up 10 years after the radiotherapy.

Conclusion: We observed a rare abscopal effect in a site distant from the area of irradiation. Irradiation of the mediastinum resulted in tumor mass regression in the untreated lung tumor.

Introduction

An abscopal effect has been defined as a reaction outside an irradiated area but within the same organism [1], that can result in a tumor in a non-irradiated area being spontaneously reduced. Since the first report of an abscopal effect by Mole in 1953 [2], several other cases have been reported in malignant lymphoma [3-5], hepatocellular carcinoma (HCC) [6] and malignant melanoma [7]. In 2007, Takaya *et al.* described an abscopal effect in a case of toruliform para-aortic lymph node metastasis in a patient with advanced uterine cervical carcinoma. This patient was treated with external whole-pelvis and intra-cavitary irradiation to the primary pelvic lesion, successfully resulting in disappearance of the lesion. Moreover, para-aortic lymph node metastases outside the irradiated field also spontaneously disappeared [8].

The mechanism of the abscopal effect has not been clearly defined. We report here the case of a patient who showed an abscopal effect on lung metastases of HCC.

Case presentation

A Japanese man, who had been followed since 53 years of age by the respiratory department of our Medical Center due to bronchial asthma, was hospitalized for progression of asthma at 63 years old. A suspected diagnosis of HCC in his right liver lobe was confirmed by abdominal computed tomography (CT). An extended right lobectomy was performed after three months in our hospital. Pathologic examination revealed an HCC, composed of a necrotic tumor that measured 10.5 × 9 × 11 cm. In addition, there were three daughter nodules with diameters of less than 1 cm each. The residual nodular tumor without necrosis was Edmondson grade II to III with nuclear atypia, and was moderately differentiated. Invasion of lymphatic and vascular channels was not obvious. Exposure to the surface of the liver

* Correspondence: yamashitah-rad@h.u-tokyo.ac.jp
[1]Department of Radiation Oncology, University of Tokyo Hospital, 7-3-1 Hongo, Bunkyo-ku, Tokyo 113-8655, Japan
Full list of author information is available at the end of the article

capsule was not found. A single lung metastasis and a single mediastinal lymph node metastasis were found in a chest CT scan performed 18 months after the liver lobectomy (Figures 1 and 2). Final diagnosis was made based on the elevated levels of two tumor markers for HCC: α-fetoprotein (AFP) (4869 ng/mL) and protein induced by vitamin K absence or antagonists II (PIVKA-II) (>20,000 mAU/mL). Trans-catheter arterial embolization for the mediastinal tumor was attempted, however the risk of spinal artery embolism resulted in the decision to only examine the tumor at that time.

Our patient was admitted to our Department of Radiation Oncology for irradiation. His Karnofsky performance status score was 90% to 100%. He complained of a moderate cough and moderate bloody sputum but denied any dyspnea or chest pain. To relieve these clinical symptoms, external-beam irradiation, with a dose of 2.25 Gy per fraction, was performed using an anteroposterior parallel-opposed technique (total dose, 60.75 Gy) (Figures 3 and 4). The energy was 10 megavolts. The radiation field was set for gross tumor volume plus a margin of 1 cm. The field size was 8 × 10 cm. Radiation therapy was given four times a week. After 40 Gy, the radiation field was changed to left-right parallel-opposed beams to spare the spinal cord (Figure 5). The lung metastasis that had induced no clinical symptoms was not treated with radiation therapy, and was located outside the radiation field of the left-right opposing beams (Figure 6). A CT scan was performed after the radiation therapy, which showed a remarkable reduction in the mediastinal lymph node. Additionally, shrinking of the tumor in his right lower lobe, outside of the radiation field, was observed (Figures 7 and 8). No chemotherapy had been given during this period.

During follow-up as an out-patient, our patient was observed to have dyspnea (Hugh-Jones 1-2), slight cough and slight sputum. AFP levels had decreased to 23 ng/mL, and PIVKA-II to 13 mAU/mL.

Figure 1 Chest CT image before radiation therapy. A bulky mediastinal lymph node metastasis was detected.

Figure 2 Two lung metastases.

A CT scan performed four years after the radiation therapy showed a lymph node swelling with a diameter of 3.5 cm in the area of origin of the left gastric artery. At this time, AFP and PIVKA-II were elevated to 1990 ng/mL and 1990 mAU/mL respectively, but with no pathologic evidence of recurrence. Stereotactic body radiotherapy for the lesion was performed, with 30 Gy in three fractions. The recurrent tumor disappeared. Six and a half months after the stereotactic body radiotherapy, no obvious recurrent disease was found.

Discussion

Many case reports describing spontaneous regression of HCC can be found in the literature. Since 1982, about 60 cases have been reported as abscopal effects or spontaneous regressions. These cases were reviewed by Oquiñena *et al.* in 2009 [9]. Although many similar reports have been published [3,4,6-8,10], the abscopal

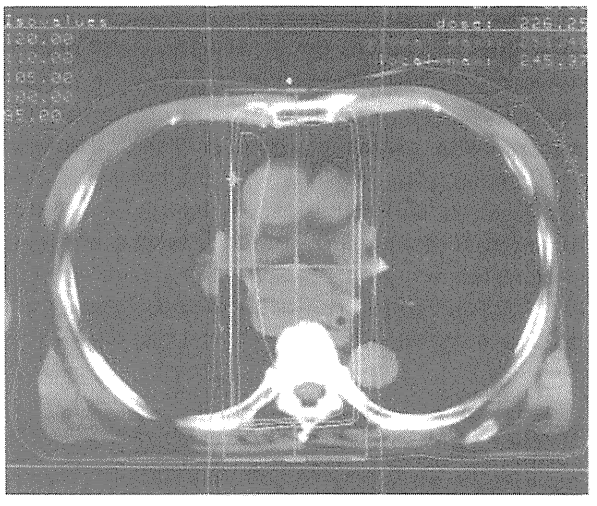

Figure 3 Chest CT image showing radiation dose distribution: axial view.

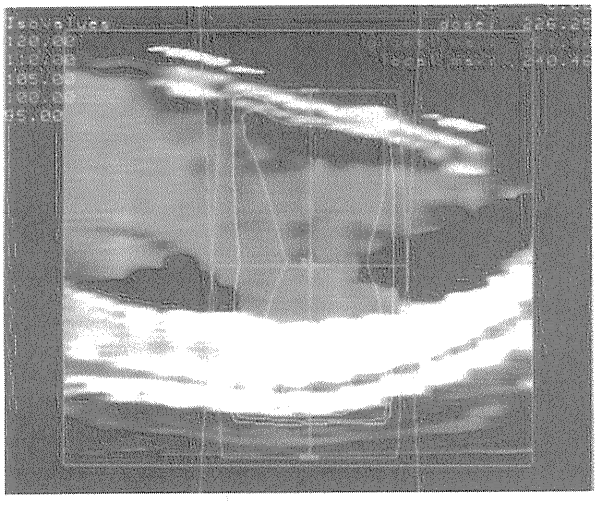

Figure 4 Chest CT image showing the radiation dose distribution: sagittal view.

effect is still a rare phenomenon, and the mechanism has not been clearly defined. Lin *et al.* proposed two mechanisms involving ischemia and an immune response [11]. First, mitotic inhibitors (cytokines) induced by local radiation are released into the circulation and mediate a systemic anti-tumor effect. This hypothesis is supported by reports that circulating tumor necrosis factor levels are elevated after radiotherapy, and have coincided with the regression of an HCC situated away from the radiation field [2,12]. Second, irradiation of a tumor in one site induces the release of circulating tumor antigen or inflammatory factors, which may then mediate an augmented immune response against non-irradiated, malignant lesions expressing similar tumor antigens. It has previously been shown that local radiotherapy increases the activity of natural killer cells [13,14]. Dewan *et al.* presented the hypothesis that the type of dose fractionation regimen determines the ability of radiotherapy to synergize with anti-CTLA-4 antibody [15]. Although these hypotheses have some merit, at present they remain to be confirmed.

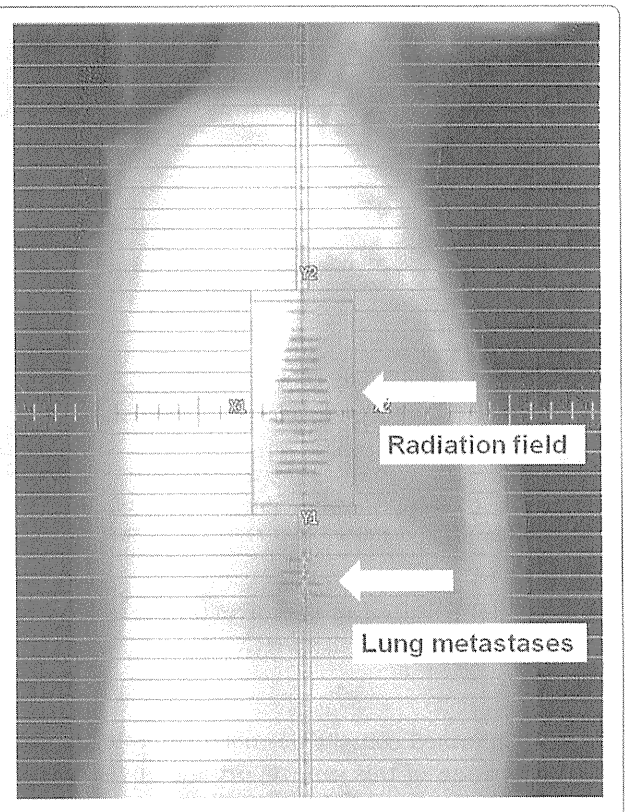

Figure 6 Beam's eye view of the lateral beam of the radiation therapy. This shows the metastatic lung tumor is outside the target area.

Conclusion

We observed a rare abscopal effect in a site distant from the area of irradiation. Irradiation of a tumor in the

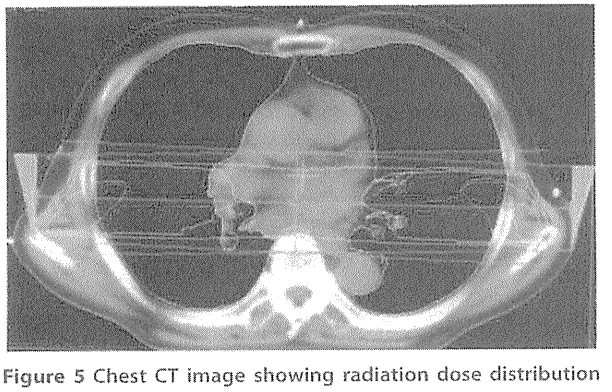

Figure 5 Chest CT image showing radiation dose distribution after 40 Gy.

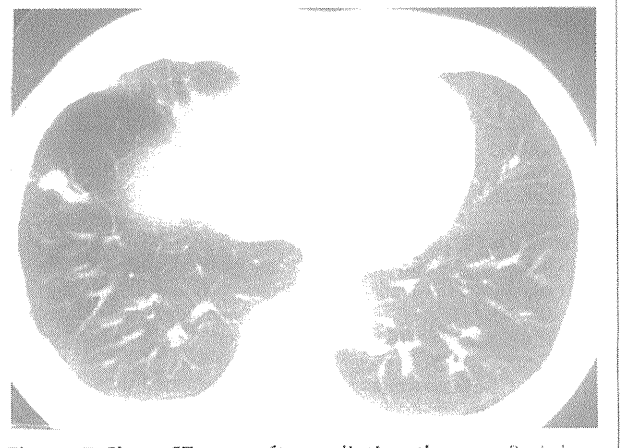

Figure 7 Chest CT scan after radiation therapy. Both lung metastases had shrunk under radiation therapy.

Figure 8 CT scan showing the absence of both lung metastases, which regressed after radiation therapy.

mediastinal resulted in tumor mass regression in an untreated lung metastasis of HCC.

Consent

Written informed consent was obtained from the patient for publication of this case report and any accompanying images. A copy of the written consent is available for review by the Editor-in-Chief of this journal.

Author details

[1]Department of Radiation Oncology, University of Tokyo Hospital, 7-3-1 Hongo, Bunkyo-ku, Tokyo 113-8655, Japan. [2]Department of Radiation Oncology, Kitasato School of Medicine, 1-15-1, Kitasato, Minami-ku, Sagamihara, Kanagawa 252-0375, Japan.

Authors' contributions

KO undertook the gathering of information for this case and was a major contributor in writing the manuscript. HY conceived the manuscript and was a major contributor to the manuscript. All authors read and approved the final manuscript.

Competing interests

The authors declare that they have no competing interests.

Received: 19 May 2010 Accepted: 19 March 2011
Published: 19 March 2011

References

1. Niibe Y, Hayakawa K: **Oligometastases and oligo-recurrence: the new era of cancer therapy.** *Jpn J Clin Oncol* 2010, 40(2):107-111.
2. Mole RH: **Whole body irradiation: radiobiology or medicine?** *Br J Radiol* 1953, 26(305):234-241.
3. Nobler MP: **The abscopal effect in malignant lymphoma and its relationship to lymphocyte circulation.** *Radiology* 1969, 93(2):410-412.
4. Antoniades J, Brady LW, Lightfoot DA: **Lymphangiographic demonstration of the abscopal effect in patients with malignant lymphomas.** *Int J Radiat Oncol Biol Phys* 1977, 2(1-2):141-147.
5. Rees GJ: **Abscopal regression in lymphoma: a mechanism in common with total body irradiation?** *Clin Radiol* 1981, 32(4):475-480.
6. Ohba K, Omagari K, Nakamura T, Ikuno N, Saeki S, Matsuo I, Kinoshita H, Masuda J, Hazama H, Sakamoto I, Kohno S: **Abscopal regression of hepatocellular carcinoma after radiotherapy for bone metastasis.** *Gut* 1998, 43(4):575-577.
7. Kingsley DP: **An interesting case of possible abscopal effect in malignant melanoma.** *Br J Radiol* 1975, 48(574):863-866.
8. Takaya M, Niibe Y, Tsunoda S, Jobo T, Imai M, Kotani S, Unno N, Hayakawa K: **Abscopal effect of radiation on toruliform para-aortic lymph node metastases of advanced uterine cervical carcinoma--case report.** *Anticancer Res* 2007, 27(1B):499-504.
9. Oquiñena S, Iñarrairaegui M, Vila JJ, Alegre F, Zozaya JM, Sangro B: **Spontaneous regression of hepatocellular carcinoma: three case reports and a categorized review of the literature.** *Dig Dis Sci* 2009, 54(5):1147-1153.
10. Lakshmanagowda PB, Viswanath L, Thimmaiah N, Dasappa L, Supe SS, Kallur P: **Abscopal effect in a patient with chronic lymphocytic leukemia during radiation therapy: a case report.** *Cases J* 2009, 2:204.
11. Lin TJ, Liao LY, Lin CL, Shih LS, Chang TA, Tu HY, Chen RC, Wang CS: **Spontaneous regression of hepatocellular carcinoma: a case report and literature review.** *Hepatogastroenterology* 2004, 51(56):579-582.
12. Hall E: **Radiobiology for the *Radiologist*.** Philadelphia: Lippincott, Williams and Wilkins, 5 2000, 588.
13. Uchida A, Mizutani Y, Nagamuta M, Ikenaga M: **Effects of X-ray irradiation on natural killer (NK) cell system. I. Elevation of sensitivity of tumor cells and lytic function of NK cells.** *Immunopharmacol Immunotoxicol* 1989, 11(2-3):507-519.
14. Demaria S, Ng B, Devitt ML, Babb JS, Kawashima N, Liebes L, Formenti SC: **Ionizing radiation inhibition of distant untreated tumors (abscopal effect) is immune mediated.** *Int J Radiat Oncol Biol Phys* 2004, 58(3):862-870.
15. Dewan MZ, Galloway AE, Kawashima N, Dewyngaert JK, Babb JS, Formenti SC, Demaria S: **Fractionated but not single-dose radiotherapy induces an immune-mediated abscopal effect when combined with anti-CTLA-4 antibody.** *Clin Cancer Res* 2009, 15(17):5379-5388.

doi:10.1186/1752-1947-5-111
Cite this article as: Okuma *et al.*: Abscopal effect of radiation on lung metastases of hepatocellular carcinoma: a case report. *Journal of Medical Case Reports* 2011 5:111.

J. Radiat. Res., 52, 112–113 (2011)

Cone Beam Computed Tomography Data Acquisition during VMAT Delivery with Subsequent Respiratory Phase Sorting Based on Projection Image Cross-correlation*

Keiichi NAKAGAWA[1]*, Satoshi KIDA[1], Akihiro HAGA[1], Yoshitaka MASUTANI[1], Hideomi YAMASHITA[1], Toshikazu IMAE[1], Kenichiro TANAKA[1], Kuni OHTOMO[1], Yoshio IWAI[2] and Kiyoshi YODA[2]

4D CBCT/Respiratory phase/VMAT.

To The Editor

Localization and verification of a tumor position was conventionally performed prior to radiotherapy. The present authors, in the past a few years, proposed in-treatment verification of the tumor position by simultaneously acquiring cone beam computed tomography (CBCT) data using an on-board kilovolt imaging system. Dose delivery was either rotational conformal[1)] or volumetric modulated arc therapy (VMAT).[2,3)] The resulting three-dimensional (3D) volume image was appropriate for still organs such as prostate. For respiratory moving cases such as lung tumors, image blurring may be observed thereby reducing the accuracy of the tumor localization.

In the meantime, Sonke et al proposed four-dimensional (4D) CBCT for respiratory moving lung tumors[4)] assuming that the motion of the diaphragm correlates well with that of a lung tumor. The respiratory phase was calculated from frame-by-frame changes of projection images after enhancing diaphragm-like features on the cranio-caudal axis. Another group also published similar results later.[5)] Kavanagh et al proposed an alternative method for extracting a respiratory pattern from a set of projection images without relying on edge detection of the diaphragm position, where simple pixel value summation was employed followed by high pass filtering.[6)] Just recently, in ESTRO annual meeting, Sonke presented 4D CBCT during VMAT delivery by extending their previous 4D CBCT research for a lung tumor.[7)]

In this letter, we present our preliminary clinical 4D CBCT imaging during VMAT delivery using Elekta Synergy (Crawly, UK). As was described in our previous report,[1)] the current Synergy system does not allow simultaneous delivery of kV CBCT beams and MV rotational beams. Having known that kV portal imaging is available during MV rotational beam delivery, we developed in-house software for CBCT reconstruction by collecting all the kV portal images during gantry rotation. We have developed a new respiratory phase sorting algorithm based on image cross-correlation between adjacent two projection images. Image cross-correlation was previously used for registering a cone beam CT image with the planning CT image inside a specified region of interest while the former image was repeatedly shifted, and the patient treatment couch was displaced according to the shift vector for the highest correlation.[8)] Similarly cross-correlation between the adjacent two projection images was calculated while one of the images was shifted stepwise, and the shift vector giving the highest correlation was considered as the tumor displacement caused by breathing. In this algorithm edge detection is not employed and the image cross-correlation is an integral operation; in other words, it is less sensitive to image noise and diaphragm may not be required in the projection image.

Figures 1(a)–(e) show kV CBCT images of a lung tumor patient during VMAT delivery in four different respiratory phases: (a) reference 3D CBCT, (b) maximum exhalation, (c) mid inhalation, (d) maximum inhalation, and (e) mid exhalation. The cross lines indicate the isocenter. 2D image data were acquired during 2 minute, half gantry rotation with 652 projections. The number of bin was selected as four in this preliminary study to obtain a reasonable image contrast to noise ratio. The 4D image indicates that the tumor size is approximately 35 mm in the cranio-caudal direction, while the tumor size is detected as approximately 42 mm with 3D CBCT. In addition, it is found from 4D CBCT that the tumor movement amplitude is approximately 9 mm in the cranio-caudal direction.

In conclusion, we have shown that 4D CBCT data acqui-

*Corresponding author: Phone: +81-3-5800-9002,
Fax: +81-3-5800-8786,
E-mail: k-nak@fg7.so-net.ne.jp

[1]Department of Radiology, University of Tokyo Hospital, 7-3-1 Hongo Bunkyo-ku, Tokyo 113-8655, Japan; [2]Elekta, KK, 3-9-1 Shibaura, Minato-ku, Tokyo 108-0023, Japan.

Conflict of interest statement: Dr. Nakagawa receives research funding from Elekta.
doi:10.1269/jrr.10170

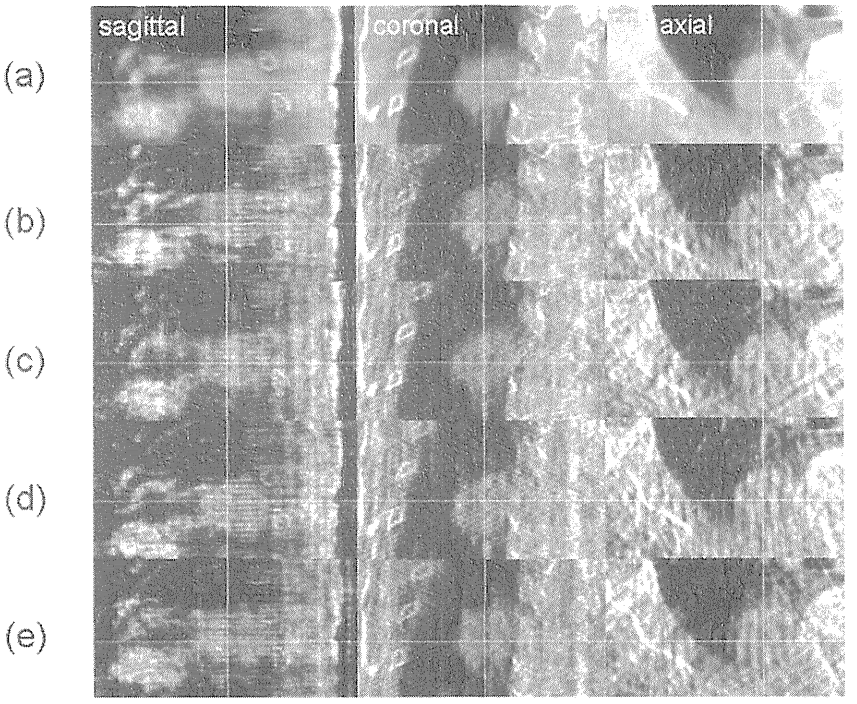

Fig. 1. kV 4D CBCT images of a lung tumor patient during VMAT delivery in four different respiratory phases: (a) reference 3D CBCT, (b) maximum exhalation, (c) mid inhalation, (d) maximum inhalation, and (e) mid exhalation. The cross lines indicate the isocenter. 2D image data were acquired during 2 minute, half gantry rotation with 652 projections. The 4D image indicates that the tumor size is approximately 35 mm in the cranio-caudal direction, while the tumor size is detected as approximately 42 mm with 3D CBCT. In addition, it is found from 4D CBCT that the tumor movement amplitude is approximately 9 mm in the cranio-caudal direction.

sition is feasible during VMAT delivery. Our respiratory phase sorting algorithm is different from previous ones and quantitative performance evaluation using large number of clinical cases is under consideration.

REFERENCES

1. Nakagawa K, *et al* (2007) Verification of in-treatment tumor position using kilovoltage cone-beam computed tomography: a preliminary study. Int J Radiat Oncol Biol Phys **69**: 970–973.
2. Nakagawa K, *et al* (2009) First clinical cone-beam CT imaging during volumetric modulated arc therapy. Radiother Oncol **90**: 422–423.
3. Nakagawa K, *et al* (2009) First report on prostate displacements immediately before and after treatment relative to the position during VMAT delivery. Acta Oncol **48**: 1206–1208.
4. Sonke JJ, *et al* (2005) Respiratory correlated cone beam CT. Med Phys **32**(4): 1176–1186.
5. Dietrich L, *et al* (2006) Linac-integrated 4D cone beam CT: first experimental results, Phys Med Biol **51**: 2939–2952
6. Kavanagh A, *et al* (2009) Obtaining breathing patterns from any sequential thoracic x-ray image set. Phys Med Biol **54**: 4879–4888
7. Sonke JJ, Remeijer P and van Herk M (2010) Four dimensional cone beam CT acquisition concurrent with VMAT delivery. Radiother Oncol **96**: **Suppl 1**, S75.
8. Sykes JR, *et al* (2005) A feasibility study for image guided radiotherapy using low dose, high speed, cone beam X-ray volumetric imaging. Radiother Oncol **77**: 45–52.

Received on December 4, 2010
Accepted on December 20, 2010

Int. J. Radiation Oncology Biol. Phys., Vol. ■, No. ■, pp. 1–7, 2011

0360-3016/$ - see front matter

ELSEVIER

doi:10.1016/j.ijrobp.2011.01.008

CLINICAL INVESTIGATION

PHASE I STUDY OF CONCURRENT HIGH-DOSE THREE-DIMENSIONAL CONFORMAL RADIOTHERAPY WITH CHEMOTHERAPY USING CISPLATIN AND VINORELBINE FOR UNRESECTABLE STAGE III NON–SMALL-CELL LUNG CANCER

IKUO SEKINE, M.D., PH.D.,* MINAKO SUMI, M.D.,PH.D.,† YOSHINORI ITO, M.D.,† HIDEHITO HORINOUCHI, M.D.,* HIROSHI NOKIHARA, M.D., PH.D.,* NOBORU YAMAMOTO, M.D., PH.D.,* HIDEO KUNITOH, M.D., PH.D.,* YUICHIRO OHE, M.D., PH.D.,* KAORU KUBOTA, M.D., PH.D.,* AND TOMOHIDE TAMURA, M.D.*

*Division of Internal Medicine and Thoracic Oncology, National Cancer Center Hospital, Tokyo, Japan; and †Division of Radiation Oncology, National Cancer Center Hospital, Tokyo, Japan

Purpose: To determine the maximum tolerated dose in concurrent three-dimensional conformal radiotherapy (3D-CRT) with chemotherapy for unresectable Stage III non–small-cell lung cancer (NSCLC).

Patients and Methods: Eligible patients with unresectable Stage III NSCLC, age ≥20 years, performance status 0–1, percent of volume of normal lung receiving 20 GY or more (V_{20}) ≤30% received three to four cycles of cisplatin (80 mg/m^2 Day 1) and vinorelbine (20 mg/m^2 Days 1 and 8) repeated every 4 weeks. The doses of 3D-CRT were 66 Gy, 72 Gy, and 78 Gy at dose levels 1 to 3, respectively.

Results: Of the 17, 16, and 24 patients assessed for eligibility, 13 (76%), 12 (75%), and 6 (25%) were enrolled at dose levels 1 to 3, respectively. The main reasons for exclusion were V_{20} >30% (n = 10) and overdose to the esophagus (n = 8) and brachial plexus (n = 2). There were 26 men and 5 women, with a median age of 60 years (range, 41–75). The full planned dose of radiotherapy could be administered to all the patients. Grade 3–4 neutropenia and febrile neutropenia were noted in 24 (77%) and 5 (16%) of the 31 patients, respectively. Grade 4 infection, Grade 3 esophagitis, and Grade 3 pulmonary toxicity were noted in 1 patient, 2 patients, and 1 patient, respectively. The dose-limiting toxicity was noted in 17% of the patients at each dose level. The median survival and 3-year and 4-year survival rates were 41.9 months, 72.3%, and 49.2%, respectively.

Conclusions: 72 Gy was the maximum dose that could be achieved in most patients, given the predetermined normal tissue constraints. © 2011 Elsevier Inc.

Lung cancer, Chemotherapy, Radiotherapy, High dose, Conformal.

INTRODUCTION

Approximately one third of patients with non–small-cell lung cancer (NSCLC) present with locally advanced Stage III disease at the initial diagnosis (1). Of this category, Stage IIIA disease with bulky N2 and Stage IIIB disease without pleural effusion are characterized by a large primary lesion and/or involvement of the mediastinal or supraclavicular lymph nodes. In addition, the majority of these patients have occult systemic micrometastases. Concurrent thoracic radiotherapy and chemotherapy has been the standard care for these patients with unresectable disease (2, 3). A platinum doublet with a third-generation anticancer agent combined with thoracic radiotherapy was reported to yield a median overall survival time (OS) of more than 2 years and long-term survivors (4–6), but the effect of platinum-based chemotherapy has reached a plateau.

The failure pattern in patients with Stage III NSCLC treated by concurrent chemoradiotherapy was roughly local recurrence alone in one third of the patients, both local and distant recurrence in another third of patients, and distant metastasis without local failure in the remaining third of patients (2, 5).

Reprint requests to: Ikuo Sekine, M.D., Ph.D., Division of Internal Medicine and Thoracic Oncology, National Cancer Center Hospital, Tsukiji 5-1-1, Chuo-ku, Tokyo 104-0045, Japan. Tel : (+81) 3-3542-2511; Fax: (+81) 3-3542-3815; E-mail: isekine@ncc.go.jp

Presented at the 45th Annual Meeting of the American Society of Clinical Oncology, May 29—June 2, 2006, Orlando, Florida.

Supported in part by Ministry of Health, Labour and Welfare, Health and Labour Science Research Grants, Research on Clinical Trials' Infrastructure Development, H21-RINKEN (Kikan)-IP-PAN-005.

Conflict of interest: none.

Acknowledgment—The authors thank Asako Sakamoto for her work as data manager and Mika Nagai for manuscript preparation.

Received June 7, 2010, and in revised form Dec 27, 2010. Accepted for publication Jan 10, 2011.

Thus, improvement of local control and suppression of distant metastasis are essential for prolongation of patient survival.

The conventional total dose of thoracic radiotherapy in patients with inoperable NSCLC has been 60 Gy administered in 30 fractions. This dose was established in 1987 by randomized Radiation Therapy Oncology Group trials that demonstrated better 3-year survival with a radiation dose of 60 Gy than with lower doses (7). In these trials, two-dimensional treatment planning was used, wherein the tumor volume was defined on kilovoltage radiographs (7). Thereafter, the standard initial target volume included the primary tumor, metastatic lymph nodes, and adjacent uninvolved ipsilateral hilar and mediastinal regions (elective nodal irradiation: ENI). Except for selected patients, excessive toxicity hampered an increase of the total dose to over 60 Gy in patients with locally advanced NSCLC.

It is, however, time now to reconsider the optimal dose of thoracic radiotherapy using new techniques in patients with locally advanced NSCLC, for the following reasons. First, positron emission tomography (PET) provides more accurate diagnosis of mediastinal lymph node metastases (8) and more accurate quantification of the tumor volumes, especially when atelectasis is present (9). Second, three-dimensional conformal radiation therapy (3D-CRT) enables radiation oncologists to delineate the tumor and adjacent normal tissue more sharply and to choose beam angles to maximize tumor coverage with minimum irradiation of normal tissues (10). Third, omission of the ENI resulted in improvement of radiation-associated toxicity without worsening the local control rate of the tumor (11, 12). Thus, by use of these new techniques, the optimal dose of thoracic radiation could exceed the conventional 60 Gy.

Two dose escalation studies in patients with locally advanced NSCLC showed that the total dose of thoracic radiotherapy could be increased up to 90 Gy in concurrent chemoradiotherapy using the 3D-CRT technique combined with weekly carboplatin and paclitaxel chemotherapy (13, 14). In these trials, chemoradiotherapy was administered after induction chemotherapy. However, it remained unclear whether these doses could be delivered safely to the majority of patients with locally advanced NSCLC, because it is not known how many patients were screened for the trials and how many of them were actually registered, and because some of the registered patients were excluded from the chemoradiotherapy phase after induction chemotherapy. The total number of patients evaluated in the two trials was also limited. Furthermore, chemotherapy other than weekly carboplatin and paclitaxel has not been evaluated in the setting of combined chemotherapy with high-dose thoracic radiotherapy, to our knowledge. The objectives of the current study were (1) to evaluate the toxicity of concurrent high-dose 3D-CRT without ENI with cisplatin and vinorelbine for unresectable Stage III NSCLC, (2) to determine the maximum tolerated dose (MTD) of thoracic radiotherapy, and (3) to observe the antitumor effects of this regimen.

PATIENTS AND METHODS

Study design

This study was designed as a Phase I study at the National Cancer Center Hospital. The protocol and consent form were approved by the Institutional Review Board of the National Cancer Center on July 28, 2005. We planned to treat 12 patients at a dose level and follow them up at least 6 months, and then escalate to the next level if 67% of the patients did not experience dose-limiting toxicity (DLT). We followed widely accepted normal tissue dose constraints. Patients with percent volume of the normal lung receiving 20 Gy or more (V_{20}) of greater than 30% were excluded and treated outside the study. Other dosimetric constraints were applied at the discretion of the treating radiation oncologist. Maximum doses exceeding 50 Gy to the spinal cord, 66 Gy to the esophagus, or 66 Gy to the brachial plexus were generally excluded.

Patient selection

Previously untreated patients with locally advanced NSCLC without effusion were screened for entry into this study. The eligibility criteria were (1) histologically or cytologically proven NSCLC, (2) unresectable Stage IIIA or IIIB disease confirmed by both computed tomography (CT) and PET, (3) no previous treatment, (4) measurable disease, (5) $V_{20} \leq 30\%$, (6) age ≥ 20 years, (7) Eastern Cooperative Oncology Group performance status (PS) of 0 or 1, and (8) adequate bone marrow function (white blood cell [WBC] count $\geq 4.0 \times 10^9$/L, hemoglobin ≥ 9.5 g/dL, and platelet count $\geq 100 \times 10^9$/L), liver function (total bilirubin ≤ 1.5 mg/dL and transaminase ≤ 80 IU/L), renal function (serum creatinine ≤ 1.5 mg/dL), and pulmonary function ($PaO_2 \geq 70$ Torr under room air). Patients were excluded if (1) they had malignant pleural or pericardial effusion or (2) they had a concomitant serious illness such as uncontrolled angina pectoris, myocardial infarction in the previous 3 months, heart failure, uncontrolled diabetes mellitus, uncontrolled hypertension, interstitial pneumonitis or lung fibrosis identified by a chest x-ray, infection, or other diseases contraindicating chemotherapy or radiotherapy, or (3) they were pregnant or breast feeding. All patients gave their written informed consent.

Pretreatment evaluation

The pretreatment assessment included a complete blood cell count and differential count, routine chemistry determinations, creatinine clearance, blood gas analysis, electrocardiogram, lung function testing, chest x-rays, chest CT scan, brain CT scan or magnetic resonance imaging, abdominal CT, and PET.

Treatment schedule

Chemotherapy consisted of cisplatin 80 mg/m^2 on Day 1 and vinorelbine 20 mg/m^2 on Days 1 and 8, repeated every 4 weeks for three to four cycles. Cisplatin was administered by intravenous infusion for 60 minutes with 2,500 to 3,000 mL of intravenous fluid for hydration and prophylactic antiemetic therapy consisting of a 5-hydroxytriptamine-3 antagonist on Day 1 and a corticosteroid on Days 1 to 5. Vinorelbine, diluted in 50 mL of normal saline, was administered intravenously.

Radiation therapy started on Day 1 of the first cycle of chemotherapy and was delivered with megavoltage equipment (6–10 MV) once daily for 5 days a week. The total dose was 66 Gy in 33 fractions at level 1, 72 Gy in 36 fractions at level 2, and 78 Gy in 39 fractions at level 3. All patients underwent a 3D treatment planning CT 3 to 7 days before the start of the treatment, and the eligibility was finally confirmed based on evaluation using the

dose–volume histogram (DVH). The gross tumor volume (GTV) was defined as the primary tumor delineated on pulmonary windows of the chest CT or on the diagnostic PET scans. Atelectasis or secondary changes in the peripheral lung region of the primary tumor were not included. Metastatic lymph nodes defined as nodes of 1 cm or larger visualized on mediastinal windows of the CT images or PET-positive lymph nodes were also included in the GTV. The clinical target volume (CTV) was equivalent to the GTV. Uninvolved mediastinum or supraclavicular fossae were not included in the CTV. The planning target volume (PTV) was determined as the CTV plus 1.0 cm for the anterior, posterior, medial, and lateral margins and a 1.0 to 2.0 cm for the superior and inferior margins, taking account of setup variations and internal organ motion. The spinal cord dose was typically limited to 44 Gy, but a maximum of 50 Gy was allowed. The lung V_{20} was limited to 30% in all patients. The maximum dose to the brachial plexus and esophagus did not exceed 66 Gy. The 100% dose was prescribed to the reference point located in the central part of the PTV, and the entire PTV was covered with 95–107% of the prescribed dose principally, but variation of ±10% was allowed. Lung heterogeneity corrections using the equivalent path length algorithm were applied in all patients.

Toxicity assessment and treatment modification

Complete blood cell counts and differential counts, routine chemistry determinations, and a chest x-ray were performed once a week during the course of treatment. Toxicity was graded according to the Common Terminology Criteria for Adverse Events (CTCAE v3.0). The lung toxicity grade was defined as the highest grade among cough, dyspnea, obstruction/stenosis of airways, pneumonitis/pulmonary infiltrates, and pulmonary fibrosis in the pulmonary/upper respiratory section (15).

Vinorelbine administration on Day 8 was omitted if any of the following were noted: WBC count $<3.0 \times 10^9$/L, neutrophil count $<1.5 \times 10^9$/L, platelet count $<100 \times 10^9$/L, Grade 2–3 elevation of the serum hepatic transaminase level or total serum bilirubin levels, Grade 2–3 infection, Grade 2–3 pneumonitis, other ≥Grade 3 nonhematologic toxicity, body temperature ≥38°C, or PS of 2–3. Subsequent cycles of cisplatin and vinorelbine chemotherapy were delayed if any of the following toxicities were noted on Day 1: WBC count $<3.0 \times 10^9$/L, neutrophil count $<1.5 \times 10^9$/L, platelet count $<100 \times 10^9$/L, serum creatinine level ≥1.6 mg/dL, Grade 2–3 elevation of the serum hepatic transaminase level or total serum bilirubin levels, Grade 2–3 infection, Grade 2–3 pneumonitis, other ≥Grade 3 nonhematologic toxicity, body temperature ≥38°C, or PS of 2–3. If these toxicities did not recover within 6 weeks from Day 1 of the previous cycle of chemotherapy, subsequent cycles of chemotherapy were stopped. The dose of cisplatin was reduced by 25% in all subsequent cycles if the serum creatinine level rose to 2.0 mg/dL or higher. The dose of vinorelbine was reduced by 25% in all subsequent cycles if any of the following toxicities were noted: WBC count $<1.0 \times 10^9$/L, platelet count $<25 \times 10^9$/L, or Grade 3 infection or liver dysfunction. Thoracic radiotherapy was suspended if any of the following were noted: body temperature ≥38°C, Grade 3 esophagitis, PS of 3, or suspected radiation pneumonitis. Thoracic radiotherapy was terminated if any of the following were noted: Grade 4 esophagitis, Grade 3 or 4 pneumonitis, PS of 4, or duration of radiotherapy of over 62 days (level 1), 67 days (level 2), or 70 days (level 3). Any protocol-defined treatments were terminated if Grade 4 nonhematologic toxicities other than transient electrolyte disturbances or a PS of 4 was noted.

Dose-limiting toxicity and maximum tolerated dose

The DLT was defined as the following toxicities observed during a 6-month period from the start of treatment: (1) Grade 3 esophagitis, lung toxicity, myelitis, dermatitis associated with radiation, and cardiac toxicity associated with radiation, (2) Grade 4 nonhematologic toxicity, or (3) treatment termination due to prolonged toxicity. Twelve patients were enrolled at each dose level. All patients were followed up for at least 6 months to evaluate DLT. During the period, if none to 4 of the 12 patients experienced DLT, the next cohort of patients was treated at the next higher dose level. If 5 or more of the 12 patients experienced DLT, that level was considered to be the MTD. The recommended dose for Phase II trials was defined as the dose preceding the MTD.

Response evaluation

Objective tumor response was evaluated according to the Response Evaluation Criteria in Solid Tumors (RECIST) ver. 1.0 (16).

Follow-up

Patients who completed the protocol therapy were followed up to monitor toxicity, response, and recurrence. CT of the chest was performed every 2 to 4 months for 1 year, every 6 months for 2 years, and then yearly for 2 years. The relapse pattern was categorized into (1) local alone, including relapse from the primary site or the hilar, mediastinal, or supraclavicular lymph nodes, (2) distant metastasis alone, including pleural dissemination, pleural and pericardial effusions, and distant metastases, and (3) local and distant.

Statistical analyses

Progression-free survival time (PFS) and OS were estimated by the Kaplan-Meier method. The PFS was measured from the date of registration to the date of disease progression or death resulting from any cause or date of last follow-up. The OS was measured from the date of registration to the date of death resulting from any cause or date of last follow-up. Patients who were lost to follow-up without events were censored at the date of their last known follow-up. A confidence interval (CI) for the response rate was calculated by the method used for exact binomial CIs. The Dr. SPSS II 11.0 software package for Windows (SPSS Japan Inc., Tokyo, Japan) was used for the statistical analyses.

RESULTS

Registration and characteristics of the patients

From August 2005 to September 2008, 57 patients were deemed to initially be eligible. Of these, 3 patients were excluded because idiopathic interstitial pneumonitis ($n = 1$) and anemia ($n = 2$) developed. Explanation of the study using the consent form was given to 54 patients, and informed consent was obtained in 51 patients. The 51 patients underwent 3D treatment planning, and eligibility was finally confirmed in 31 patients. Those 31 were enrolled into this study. A total of 20 patients were excluded as a result of the DVH evaluation: because of V_{20} higher than 30% in 10 patients, overdose to the esophagus in 8 patients, and overdose to the brachial plexus in 2 patients. Eventually, of 17 patients assessed as to their eligibility for dose level 1, 16 patients for dose level 2, and 24 patients to dose level 3, 13 (76%), 12 (75%), and 6 (25%) patients were actually enrolled into levels 1 to 3, respectively (Fig. 1).

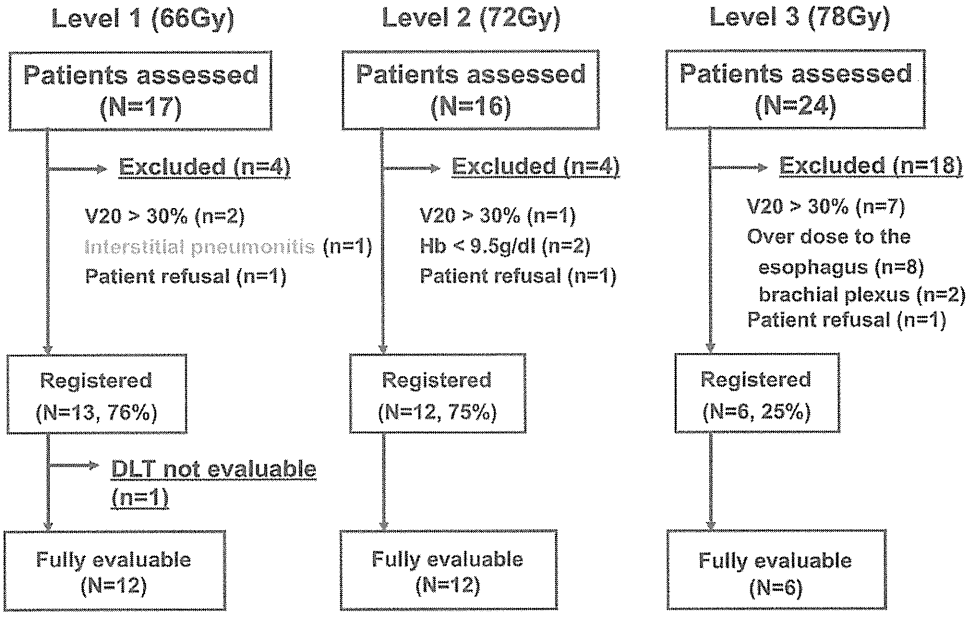

Fig. 1. Algorithm illustrating the flow of the patients. Of the 17, 16, and 24 patients assessed for eligibility, 13 (76%), 12 (75%), and 6 (25%) were actually enrolled at dose levels 1, 2, and 3, respectively.

The pretreatment characteristics of the patients enrolled in this trial are shown in Table 1. The majority of the patients were in good general condition, with a PS of 0 in 25 (81%) and no weight loss in 26 (84%) patients. Adenocarcinoma was the predominantly encountered histological characteristic, seen in 23 (74%) patients.

Treatment delivery

The treatment delivery to the patients was fairly good (Table 2). The planned dose of radiotherapy was administered to all patients of all the three dose levels. More than 80% of the patients received three to four cycles of chemotherapy without or with only one omission of vinorelbine on Day 8, regardless of the dose levels.

Toxicity and DLTs

The hematologic toxicity was comparable to that of other concurrent chemoradiotherapy (Table 3). Grade 4 septic shock was encountered during the fourth cycle of chemotherapy in 1 patient enrolled at dose level 1, but it was manageable by standard care with antibiotics. Other nonhematologic toxicities were mild and acceptable.

Table 1. Patient characteristics

Characteristic	*n*	(%)
Sex		
M	26	(84)
F	5	(16)
Age (y)		
Median (range)	60	(41–75)
Performance status		
0	25	(81)
1	6	(19)
Body weight loss (%)		
0	26	(84)
0.1–5.0	2	(6)
≤5.0	3	(10)
Histology		
Adenocarcinoma	23	(74)
Squamous cell carcinoma	4	(13)
NSCLC, not otherwise specified	4	(13)
Stage		
IIIA	20	(65)
IIIB	11	(35)

Abbreviation: NSCLC = non–small-cell lung cancer.

Table 2. Treatment delivery

	Level 1 (*n* = 13)	Level 2 (*n* = 12)	Level 3 (*n* = 6)
Radiotherapy			
Total dose (Gy)			
66	13 (100)	–	–
72	–	12 (100)	–
78	–	–	6 (100)
Delay (days)			
≤5	11 (85)	5 (42)	5 (83)
6–10	2 (15)	6 (50)	0
11–15	0	1 (8)	1 (17)
Chemotherapy			
No. of cycles			
4	6 (46)	6 (50)	4 (67)
3	6 (46)	4 (33)	2 (33)
2	0	1 (8)	0
1	1 (8)	1 (8)	0
No. of VNR omissions			
0	10 (77)	7 (58)	2 (33)
1	2 (15)	4 (33)	3 (50)
2	0	0	1 (17)
3	1 (8)	1 (8)	0

Abbreviation: VNR = vinorelbine administered on Day 8.

Table 3. Toxicity

	Grade										
	Level 1			(n = 13)	Level 2			(n = 12)	Level 3			(n = 6)
Toxicity	2	3	4	(3+4 %)	2	3	4	(3+4 %)	2	3	4	(3+4 %)
Leukopenia	4	6	2	(62)	1	3	8	(92)	1	3	2	(83)
Neutropenia	4	4	4	(62)	0	1	10	(92)	1	3	2	(83)
Anemia	8	2	2	(31)	7	3	1	(33)	2	2	0	(50)
Thrombocytopenia	0	0	0	(0)	1	1	0	(8)	0	0	0	(0)
Febrile neutropenia	–	1	0	(8)	–	3	0	(25)	–	1	0	(17)
Infection	0	0	1	(8)	0	1	0	(8)	2	0	0	(0)
Esophagitis	1	1	0	(8)	2	1	0	(8)	0	0	0	(0)
Lung toxicity	2	0	0	(0)	0	0	0	(0)	0	1	0	(17)
Anorexia	3	0	0	(0)	2	2	0	(17)	0	0	0	(0)
Nausea	3	0	0	(0)	3	0	0	(0)	0	0	0	(0)
ALT elevation	1	1	0	(8)	0	0	0	(0)	1	0	0	(0)
CRN elevation	7	0	0	(0)	4	0	0	(0)	0	0	0	(0)

Abbreviations: ALT = alanine aminotransferase; CRN = creatinine.

Of the 13 patients at dose level 1, one was excluded from the analysis of the DLT because he received only one cycle of chemotherapy as a result of the development of cisplatin-induced renal toxicity. Two (17%) of the remaining 12 patients at this dose level developed DLT: Grade 3 esophagitis in 1 patient and Grade 4 septic shock in the other. At dose level 2, two (17%) DLTs were noted: Grade 3 esophagitis in 1 patient and treatment delay by more than 15 days in the other. One (17%) of the 6 patients at dose level 3 developed Grade 3 bronchial stenosis without local recurrence of the disease. This was considered to be a Grade 3 lung toxicity and was counted as DLT. No other DLTs were noted. Thus, inasmuch as the incidence of DLT was below 33% at all dose levels, MTD was not reached.

Preliminary efficacy results

Objective responses and survival were evaluated in the 31 patients. Two patients showed complete responses and 27 showed partial responses, which represented a response rate (95% CI) of 94% (79–99). Disease progression was noted in 23 patients, and the median PFS was 11.6 months with a median duration of follow-up of 30.5 (range, 9.0–49.5) (Fig. 2). The first relapse sites aresummarized in Table 4. Brain metastasis alone as the first relapse site was noted in 7 (23%) patients. The median OS was 41.9 months, and the 2-, 3-, and 4-year survival rates (95% CI) were 83.6% (65.0–92.8), 72.3% (51.9–85.2), and 49.2% (26.2–68.7), respectively (Fig. 3).

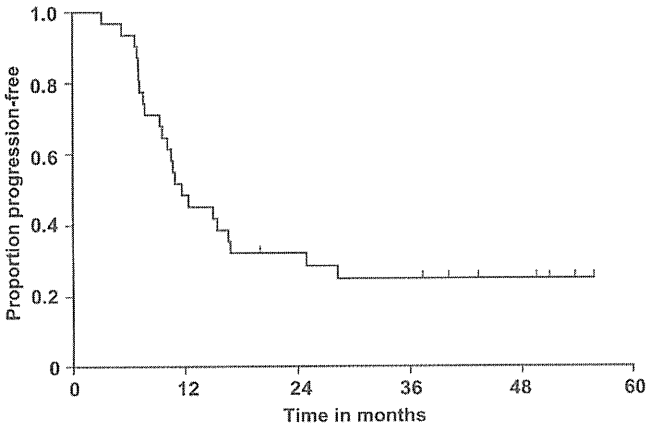

Fig. 2. Progression-free survival (n = 31). The median progression-free survival was 11.6 months, with a median duration of follow-up of 30.5 months (range, 9.0–49.5 months).

DISCUSSION

This study showed that concurrent 3D-CRT to the thorax with cisplatin plus vinorelbine chemotherapy was safe even up to 78 Gy in patients with unresectable Stage III NSCLC. This does not mean, however, that doses as high as 78 Gy can be given to all patients with this disease, because the safety in this study was shown only in highly selected patients by a PET/CT and DVH evaluation and by the standard staging procedure. Twenty-five of the 33 patients met the eligibility criteria for enrollment at dose levels 1 and 2, whereas only 6 of the 24 patients could be enrolled at dose level 3 in this study—that is, only one fourth of the patients could be treated with 78 Gy. Thus, this study showed that 72 Gy was the maximum dose that could be achieved in most patients given the predetermined normal tissue constraints, which forced three quarters of the enrolled patients at the 78-Gy level to not be eligible on the basis of those normal

Table 4. First relapse sites (n = 31)

Sites	n	(%)
Local recurrence alone	6	(19)
Local and distant metastasis	6	(19)
Distant metastasis alone	11	(35)
Brain alone	7	(23)
No relapse	8	(26)

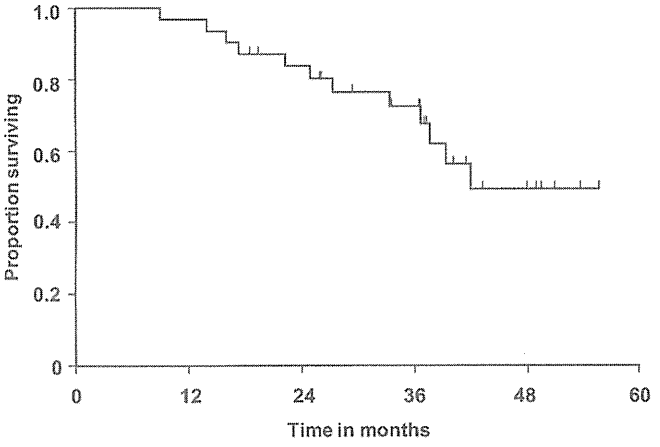

Fig. 3. The median overall survival was 41.9 months, and the 2-, 3-, and 4-year survival rates (95% CI) were 83.6% (65.0–92.8), 72.3% (51.9–85.2), and 49.2% (26.2–68.7), respectively.

tissue constraints, and that the maximum tolerated dose was not determined because of this issue.

One obstacle to enrolling patients at dose level 3 was that the lung V_{20} often exceeded 30% when the total dose was increased to 78 Gy. This lung V_{20} dose constraint might have been too strict. According to a recent review, it is prudent to limit V_{20} to ≤30–35% with conventional fractionation, but there is no sharp dose threshold below which there is no risk for severe radiation pneumonitis (17). This is partly because DVH-based parameters will change at specific phases of the respiratory cycle when CT images for DVH evaluation have been obtained, there is uncertainty regarding how much of the bronchus should be defined as lung, and the lung edges may vary with the CT window level setting. In addition, patient-associated factors such as age, smoking status, lung function, and preexisting lung damage may influence the incidence and severity of radiation pneumonitis (18). If the threshold of V_{20} were set at higher than 30% (*e.g.*, 35%), then more patients would meet the eligibility criteria, but safety might not be guaranteed. Given that the definite threshold cannot be determined, a strict constraint should be introduced. This study showed that the lung toxicity was acceptable when the V_{20} was kept within 30%; therefore, we decided to use this eligibility criterion for concurrent chemotherapy and high-dose radiotherapy for a subsequent Phase II study.

Another obstacle was overdose to the esophagus and brachial plexus, which were close to the subcarinal (No. 7) and supraclavicular lymph nodes, respectively, that were frequently involved in patients with advanced NSCLC; therefore, the volume of these serial organs were included, in part, in the PTV in many patients with Stage III disease. The radiation tolerance doses of these organs have been defined as no higher than 72 Gy when one third of the organs are included in the irradiation volume (19). However, few data are available on the radiation tolerance doses of normal organs in humans; therefore, whether or not radiation doses above 72 Gy may be tolerated is unknown, especially when only small percentages of the organs are actually included in the irradiation volume. Notwithstanding, we do not agree that the radiation dose can be increased close to the intolerable level, because serious radiation toxicity to these serial organs could be irreversible, frequently leaves severe sequelae, and is fatal in some cases.

The toxicity observed in this trial was comparable to that in our previous study of concurrent chemoradiotherapy with vinorelbine and cisplatin chemotherapy plus thoracic radiation at a total dose of 60 Gy administered in 30 fractions: Grade 3–4 neutropenia in 77% and 67% of patients, Grade 3–4 esophagitis in 6% and 12% of patients, and Grade 3–5 lung toxicity in 3% and 7% in the current and previous studies, respectively (5). This suggests that patient selection using PET/CT and DVH evaluation may be useful to keep the toxicity associated with high-dose thoracic radiation within the range of toxicity induced by conventional-dose thoracic radiation.

In this study, a remarkably high proportion (74%) of subjects had adenocarcinoma, which may provide an explanation for the high rate of subsequent brain metastases. Patient selection also affects the treatment efficacy considerably; therefore, it is difficult to compare it between the current and previous studies. However, the median PFS of 11.6 months and median OS of 41.9 months sound promising. We are conducting a Phase II study of concurrent 3D-CRT at a total dose of 72 Gy and chemotherapy with cisplatin and vinorelbine.

In conclusion, concurrent 3D-CRT with cisplatin and vinorelbine chemotherapy was feasible up to 72 Gy, in patients with unresectable Stage III NSCLC. At the level of 78 Gy, however, only 25% of the patients assessed for eligibility were found to be actually eligible. Thus, 72 Gy in 36 fractions was the maximum dose that could be achieved in most patients given the predetermined normal tissue constraints when administered concurrently with cisplatin and vinorelbine.

REFERENCES

1. Yang P, Allen MS, Aubry MC, *et al.* Clinical features of 5,628 primary lung cancer patients: Experience at Mayo Clinic from 1997 to 2003. *Chest* 2005;128:452–462.
2. Furuse K, Fukuoka M, Kawahara M, *et al.* Phase III study of concurrent versus sequential thoracic radiotherapy in combination with mitomycin, vindesine, and cisplatin in unresectable stage III non-small-cell lung cancer. *J Clin Oncol* 1999;17: 2692–2699.
3. Curran WJ, Scott C, Langer C, *et al.* Phase III comparison of sequential vs concurrent chemoradiation for patients with unresectable stage III non-small-cell lung cancer (NSCLC): Initial report of the Radiation Therapy Oncology Group (RTOG) 9410. *Proc Am Soc Clin Oncol* 2000;19: 484a.
4. Sekine I, Noda K, Oshita F, *et al.* Phase I study of cisplatin, vinorelbine, and concurrent thoracic radiotherapy for

unresectable stage III non-small cell lung cancer. *Cancer Sci* 2004;95:691–695.
5. Sekine I, Nokihara H, Sumi M, *et al.* Docetaxel consolidation therapy following cisplatin, vinorelbine, and concurrent thoracic radiotherapy in patients with unresectable stage III non-small cell lung cancer. *J Thorac Oncol* 2006;1:810–815.
6. Kiura K, Takigawa N, Segawa Y, *et al.* Randomized phase III trial of docetaxel and cisplatin combination chemotherapy versus mitomycin, vindesine and cisplatin combination chemotherapy with concurrent thoracic radiation therapy for locally advanced non-small cell lung cancer: OLCSG 0007. *J Clin Oncol* 2008;26(Suppl):400s (abstr. 7515).
7. Perez CA, Pajak TF, Rubin P, *et al.* Long-term observations of the patterns of failure in patients with unresectable non-oat cell carcinoma of the lung treated with definitive radiotherapy. Report by the Radiation Therapy Oncology Group. *Cancer* 1987; 59:1874–1881.
8. Birim O, Kappetein AP, Stijnen T, *et al.* Meta-analysis of positron emission tomographic and computed tomographic imaging in detecting mediastinal lymph node metastases in nonsmall cell lung cancer. *Ann Thorac Surg* 2005;79:375–382.
9. Nestle U, Walter K, Schmidt S, *et al.* 18F-deoxyglucose positron emission tomography (FDG-PET) for the planning of radiotherapy in lung cancer: High impact in patients with atelectasis. *Int J Radiat Oncol Biol Phys* 1999;44:593–597.
10. Purdy J. Three-dimensional conformal radiation therapy: Physics, treatment planning, and clinical aspects. In: Halperin E, Perez C, Brady L, editors. Principles and practice of radiation oncology. 5th ed. Philadelphia: Wolters Kluwer Lippincott Williams & Wilkins; 2008.
11. Rosenzweig KE, Sura S, Jackson A, *et al.* Involved-field radiation therapy for inoperable non small-cell lung cancer. *J Clin Oncol* 2007;25:5557–5561.
12. Sanuki-Fujimoto N, Sumi M, Ito Y, *et al.* Relation between elective nodal failure and irradiated volume in non-small-cell lung cancer (NSCLC) treated with radiotherapy using conventional fields and doses. *Radiother Oncol* 2009;91: 433–437.
13. Socinski MA, Morris DE, Halle JS, *et al.* Induction and concurrent chemotherapy with high-dose thoracic conformal radiation therapy in unresectable stage IIIA and IIIB non-small-cell lung cancer: A dose-escalation phase I trial. *J Clin Oncol* 2004;22: 4341–4350.
14. Rosenman JG, Halle JS, Socinski MA, *et al.* High-dose conformal radiotherapy for treatment of stage IIIA/IIIB non-small-cell lung cancer: Technical issues and results of a phase I/II trial. *Int J Radiat Oncol Biol Phys* 2002; 54:348–356.
15. Miller KL, Shafman TD, Marks LB. A practical approach to pulmonary risk assessment in the radiotherapy of lung cancer. *Semin Radiat Oncol* 2004;14:298–307.
16. Therasse P, Arbuck SG, Eisenhauer EA, *et al.* New guidelines to evaluate the response to treatment in solid tumors. European Organization for Research and Treatment of Cancer, National Cancer Institute of the United States, National Cancer Institute of Canada. *J Natl Cancer Inst* 2000;92: 205–216.
17. Marks LB, Bentzen SM, Deasy JO, *et al.* Radiation dose-volume effects in the lung. *Int J Radiat Oncol Biol Phys* 2010;76(3 Suppl):S70–S76.
18. Mehta V. Radiation pneumonitis and pulmonary fibrosis in non-small-cell lung cancer: Pulmonary function, prediction, and prevention. *Int J Radiat Oncol Biol Phys* 2005;63:5–24.
19. Emami B, Lyman J, Brown A, *et al.* Tolerance of normal tissue to therapeutic irradiation. *Int J Radiat Oncol Biol Phys* 1991; 21:109–122.